Supporting information for

Theoretical Analysis of the Relationship between Quasi-BIC and Intrinsic Parameters in Surface plasmon resonance Sensors

Xinghong Chen†, Weiyu Kong†*

Affiliations

School of Electronic Information and Electrical Engineering, Shanghai Jiao Tong University, Shanghai 200240, China.

†These authors contributed equally to this work.

Contact Information

*Correspondence to: kong_weiyu@sjtu.edu.cn

Email addresses of all authors: chenxingh@sjtu.edu.cn, kong_weiyu@sjtu.edu.cn

Content

S1. Simulation structure and setup

The simulated structure of the SPR sensor based on quasi-BICs is shown in Figure S1 (2D structure), which was computed using a commercial finite element simulator. The x-direction is set to Floquet periodic boundary conditions, and the y-direction is set to Perfectly Matched Layers (PML). The latter is designed to ensure that the electromagnetic waves at the periphery of the structure are absorbed. The simulation is initiated by a broadband plane wave as the incident light source, with an angle of incidence of θ. The direction of the electric field(E) polarization of the incident light is positioned in the x-y plane.

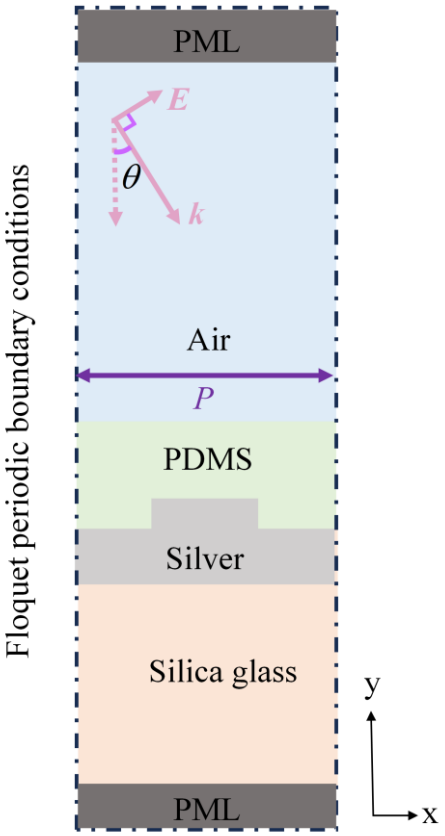

Figure S1. x-y section of the simulated structure.

S2. Spectra of quasi-BICs under different angles of incidence

The reflection spectra of the device at varying incidence angles are depicted in Figure S2(a). The green dashed circle indicates the theoretical existence of a BIC with an infinite Q-factor (symmetry-protected BIC). When the incident angle of light is

altered, the structural symmetry of the device is broken, and the BIC with an infinite Q-factor is transformed into a quasi-BICs with a finite Q-factor. This transition is accompanied by the emergence of a pronounced Fano resonance, quasi-BICs (light green area), which is attributed to the symmetry-breaking coupling between the guided mode and the radiative continuum states. The Q-factor of the quasi-BICs undergoes a decrease in conjunction with the gradual increase in the incident angle. Concurrently, the SPR mode at low wavelengths gradually transforms into the Friedrich-Wintgen BIC, as depicted in the energy band diagram of Figure 2(b) in the main text.

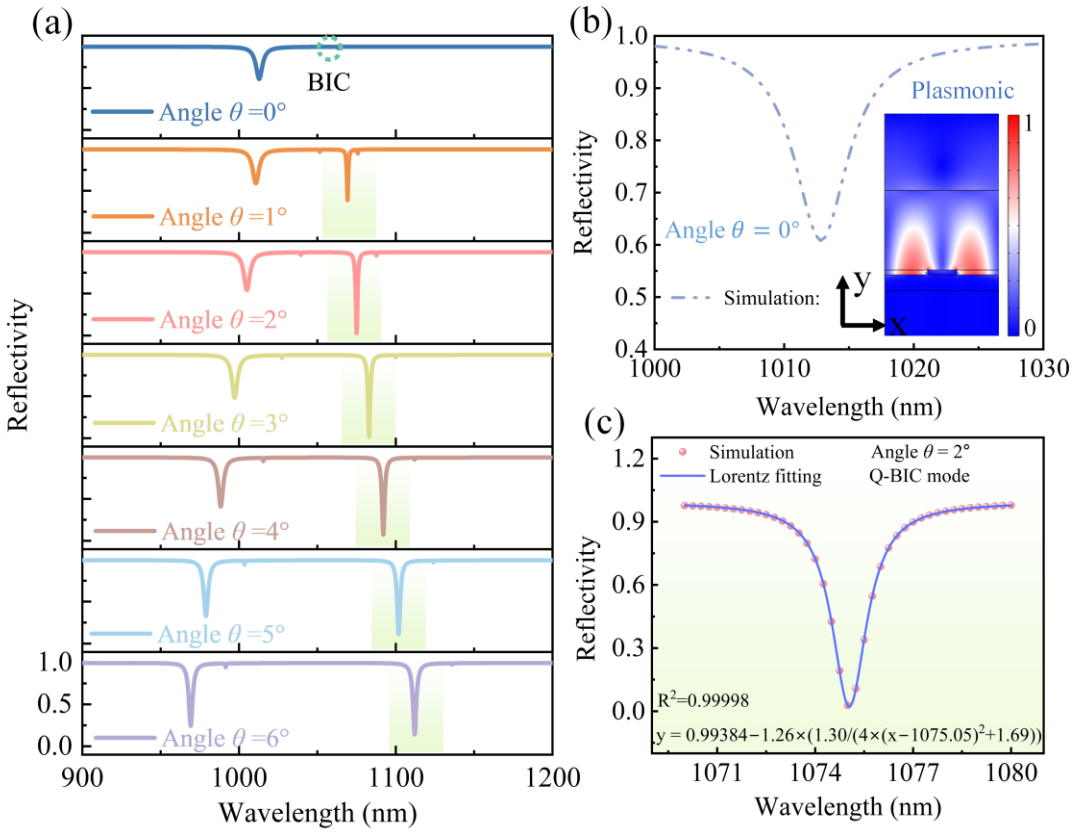

Figure S2. Reflection spectra of the device at varying angles of incidence. (a) The spectra at varying angles of incidence, accompanied by the formation of quasi-BICs. (b) The spectrum at an incident angle of 0° and the electric field distribution of the SPR mode. (c)The spectrum in quasi-BICs. The light red data points represent the simulation results, while the light blue curves correspond to the Lorentzian fitting results.

Additionally, when the angle of incidence is 0°, the spectrum of the device is shown in Figure S2(b). At this particular angle, the spectrum of the device exhibits a single SPR mode, with a resonance wavelength approaching 1010 nm. The inset illustrates

that the electric field of this SPR mode is predominantly distributed on the surface of the metallic silver film. The spectrum of the quasi-BICs ($\theta = 2°$) is depicted in Figure S2(c). The light red data points represent the simulation results. The light blue curve corresponds to the Lorentz formula fitting results, which exhibit a perfect fit, thereby demonstrating the efficacy of the Lorentz formula in accurately representing the reflection spectrum of quasi-BICs. The figure also illustrates the FWHM of the quasi-BICs at varying angles of incidence (Figure S3). As demonstrated in Figure S3(a-f), the FWHM of the quasi-BICs displays a gradual increase with the rise in the angle of incidence when the incidence is between 1−6°, thereby indicating a concomitant decrease in the Q-factor of the mode.

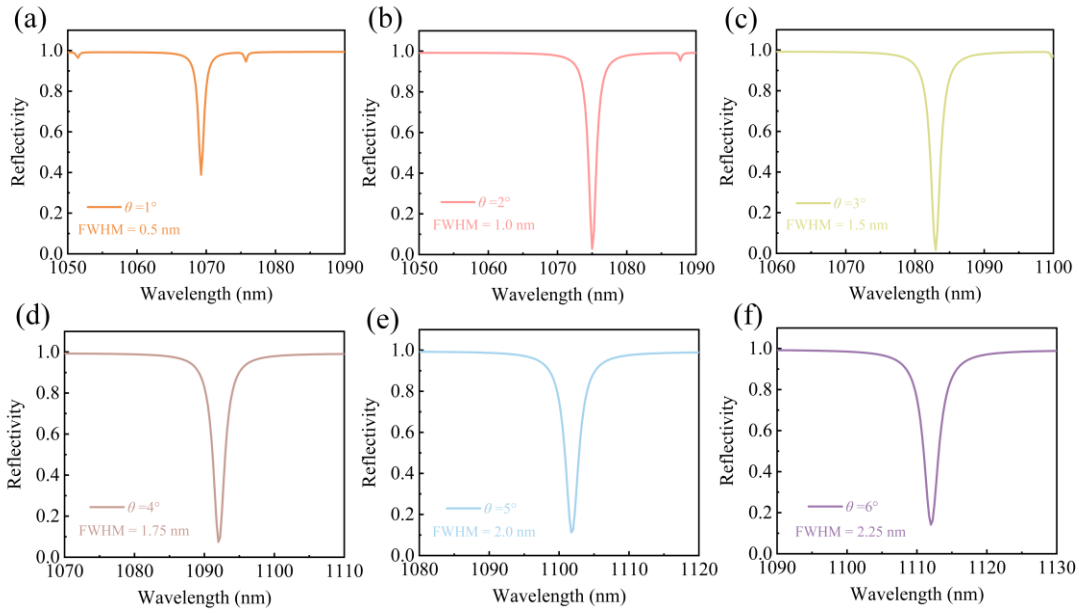

Figure S3. Spectra as well as the FWHM of quasi-BICs at varying incidence angles. (a-f) The spectra and the corresponding FWHM of quasi-BICs at different incidence angles (1−6°, with angular intervals of 1°).

S3. Spectra of quasi-BICs with different structural parameters

The effect of different structural parameters on the quasi-BICs is demonstrated in Figure S4. With all other parameters fixed at $\theta = 2°$ (a_1= 180 nm, a_2 = 270 nm, t = 130 nm, h = 100 nm), the spectra of the quasi-BICs with varying PDMS thickness (d) are displayed in Figure S4(a). The results demonstrate that the resonant wavelengths of both SPR and quasi-BICs exhibit a slight redshift when the thickness of the PDMS is gradually increased. Furthermore, when the ridge width (a_1) of the silver grating is

augmented while maintaining constant other parameters, the resonance wavelengths of both SPR and quasi-BICs undergo a red shift (Figure. S4(b)). A similar outcome was observed when the width of the gap (a_2) between the ridges of the silver gratings was gradually increased (Figure S4(c)). The aforementioned results indicate that the resonant wavelength of the quasi-BICs can be tunable by changing the period (P) of the silver grating ($P = a_1 + 2a_2$), which allows the device to operate at a wavelength that can be flexibly adapted to the photodetection system.

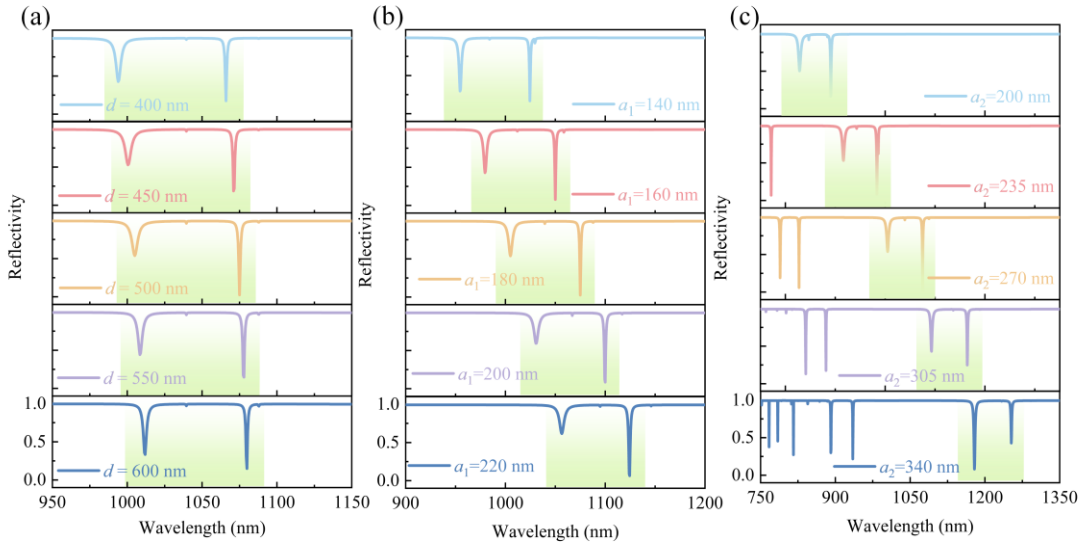

Figure S4. Different structural parameters on the spectra of the quasi-BICs (θ = 2°). (a) The spectra as a function of the thickness of the PDMS with other parameters fixed (a_1= 180 nm, a_2 = 270 nm, t = 130 nm, h = 100 nm). (b) The relationship between the spectra as a function of the silver grating ridges (a_1) with other parameters fixed (a_2 = 270 nm, t = 130 nm, h = 100 nm, d = 500 nm). (c) The relationship between the spectra as a function of the silver grating gap (a_2), with the other parameters fixed (a_1= 180 nm, t = 130 nm, h = 100 nm, d = 500 nm).

S4. Intrinsic parameters of the device at different angles of incidence and for different structural parameters

To facilitate the comparison of the performance parameters of the quasi-BIC and SPR modes of the device at different angles of incidence, please refer to Table S1, which lists the results of the comparison of the intrinsic parameters of the two modes. A comparison of the quasi-BIC with the SPR mode reveals a substantial advantage in

terms of Q factor, FOM, and intensity sensitivity. Concurrently, the wavelength sensitivity and temperature sensitivity of both modes exhibited enhanced stability, suggesting that the device's temperature performance demonstrates superior angular robustness. Furthermore, the performance parameters inherent to the quasi-BIC and SPR modes of the device under different structural parameters are shown in Tables S2, S3, and S4, respectively. The findings indicate that quasi-BIC exhibits a substantial superiority over the conventional SPR mode in terms of Q factor and FOM intensity sensitivity. Concurrently, quasi-BIC exhibits specific relative merits in terms of wavelength sensitivity and temperature sensitivity.

Table S1. Comparison of device intrinsic parameters at different incidence angles

	Angle (degree)	**Wavelength Sensitivity** (nm/RIU)	**Q-factor**	**FOM** (RIU^{-1})	**Intensity Sensitivity** (RIU^{-1})	**Temperature Sensitivity** （nm/℃）
Quasi-BIC	1	728.93	2138.5	1457.86	882.01	-0.328
	2	725.00	1075	725.00	699.84	-0.326
	3	721.07	722	480.71	469.49	-0.324
	4	717.14	624	409.79	376.57	-0.323
	5	715.00	550.88	357.50	315.03	-0.322
	6	712.14	494.22	316.51	269.83	-0.320
	Angle (degree)	**Wavelength Sensitivity** (nm/RIU)	**Q-factor**	**FOM** (RIU^{-1})	**Intensity Sensitivity** (RIU^{-1})	**Temperature Sensitivity** （nm/℃）
SPR mode	1	687.14	224.61	152.70	61.57	-0.309
	2	691.43	236.47	162.69	73.98	-0.311
	3	694.64	249.31	173.66	89.33	-0.313
	4	695.00	282.36	198.57	116.20	-0.313
	5	684.29	301.15	210.55	140.28	-0.308
	6	690.00	387.70	276.00	207.28	-0.311

Table S2. Comparison of intrinsic parameters of devices with different structural parameters (*d*)

	Parameters （nm）	**Wavelength Sensitivity** (nm/RIU)	**Q-factor**	**FOM** (RIU^{-1})	**Intensity Sensitivity** (RIU^{-1})	**Temperature Sensitivity** （nm/℃）
Quasi-BIC	*d*=400	713	1066	713	583.66	-0.321
	d =450	720	2142	1440	1158.26	-0.324
	d =500	725	1075	725	699.84	-0.326
	d =550	733	2156	1466	1258.27	-0.330
	d =600	737	2160	1474	1272.87	-0.332
	Parameters （nm）	**Wavelength Sensitivity** (nm/RIU)	**Q-factor**	**FOM** (RIU^{-1})	**Intensity Sensitivity** (RIU^{-1})	**Temperature Sensitivity** （nm/℃）
SPR mode	*d*=400	675	284	192.86	109.55	-0.304
	d =450	687	250.13	171.75	79.83	-0.309
	d =500	691.43	236.47	162.69	73.98	-0.311
	d =550	700	336.17	233.33	129.08	-0.315
	d =600	708	506	354	235.20	-0.319

Table S3. Comparison of intrinsic parameters of devices with different structural parameters (a_1)

	Parameters （nm）	**Wavelength Sensitivity** (nm/RIU)	**Q-factor**	**FOM** (RIU^{-1})	**Intensity Sensitivity** (RIU^{-1})	**Temperature Sensitivity** （nm/℃）
Quasi-BIC	a_1=140	698	1024.5	698	577.18	-0.314
	a_1=160	713	1050	713	653.46	-0.321
	a_1=180	725	1075	725	699.84	-0.326
	a_1=200	742	733.30	494.67	448.91	-0.334
	a_1=220	757	749.67	504.67	468.43	-0.341
	Parameters （nm）	**Wavelength Sensitivity** (nm/RIU)	**Q-factor**	**FOM** (RIU^{-1})	**Intensity Sensitivity** (RIU^{-1})	**Temperature Sensitivity** （nm/℃）
SPR mode	a_1=140	660	381.8	264	184.27	-0.297
	a_1=160	675	326.5	225	127.17	-0.304
	a_1=180	691.43	236.47	162.69	73.98	-0.311
	a_1=200	712	229.0	158.22	62.87	-0.320
	a_1=220	730	211.3	146	55.04	-0.329

Table S4. Comparison of intrinsic parameters of devices with different structural parameters (a_2)

	Parameters（nm）	Wavelength Sensitivity (nm/RIU)	Q-factor	FOM (RIU^{-1})	Intensity Sensitivity (RIU^{-1})	Temperature Sensitivity（nm/℃）
Quasi-BIC	a_2=200	608	594.0	405.33	333.91	-0.274
	a_2=235	669	983.5	669	618.22	-0.301
	a_2=270	725	1075	725	699.84	-0.326
	a_2=305	780	1164.5	780	578.92	-0.351
	a_2=340	830	1253	830	470.61	-0.374
	Parameters（nm）	**Wavelength Sensitivity** (nm/RIU)	**Q-factor**	**FOM** (RIU^{-1})	**Intensity Sensitivity** (RIU^{-1})	**Temperature Sensitivity**（nm/℃）
SPR mode	a_2=200	576	184.1	128	62.61	-0.259
	a_2=235	635	203.67	141.11	65.15	-0.286
	a_2=270	691.43	236.47	162.69	73.98	-0.311
	a_2=305	752	364.33	250.67	140.85	-0.338
	a_2=340	803	589.5	401.5	365.77	-0.361

S5. Electric field distribution in Quasi-BIC and SPR modes for devices containing metallic gold and silver materials

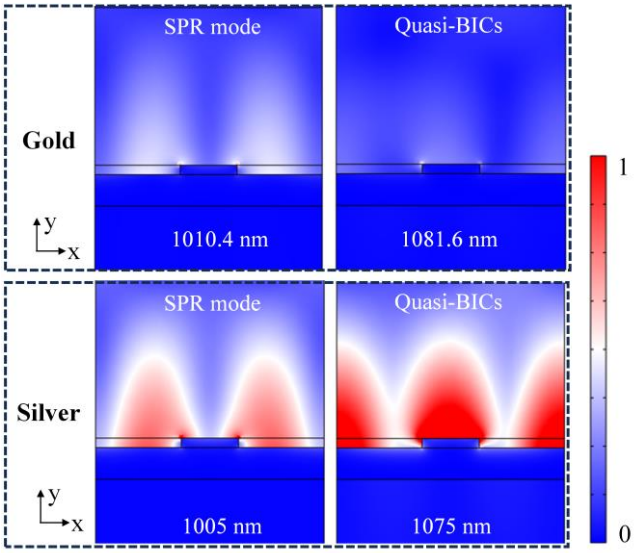

Figure S5. Field distributions of quasi-BIC and SPR modes for different metallic devices

S6. Interpretation of dλ/dn for the sensor in two modes (conventional SPR mode and Quasi-BIC)

To comprehensively study the wavelength sensitivity of the device, we set different incident angle parameters and present the simulation results for the wavelength sensitivity (dλ/dn) of the device in quasi-BIC and SPR modes, respectively. The results show that the wavelength modulation sensitivity corresponding to the quasi-BIC is approximately ~720 nm/RIU for an angular range of 1-6 degrees, while that corresponding to the SPR mode is approximately~690 nm/RIU(see Table S1). Similarly, when the structural parameters of the device were adjusted, the wavelength sensitivities of the device for both the quasi-BICs and the SPR mode were simulated. The results indicate that there is no significant difference in wavelength sensitivity between the quasi-BIC and SPR modes(see Table S2, S3,and S4). The wavelength sensitivity primarily reflects the change in the spectral resonance wavelength of the device resulting from a change in the external refractive index. In this study, the device contains a metal structure, with the mode field primarily distributed on the metal surface, which is in direct contact with the external environment. Consequently, the wavelength sensitivities of the two modes are not significantly different from each other.

S7. Interpretation of the parameters threshold (η) and wavelength interrogation noise(N_λ)

In this paper, as far as the parameter η is concerned, it is an independent value that does not have a definite correspondence with the Q-factor, FWHM, and spectral depth of the resonance spectrum. In addition, for refractive index sensing applications, the wavelength interrogation noise (N_λ) is related to both the Q factor and FWHM. In other words, a higher Q-factor, lower FWHM, and higher spectral depth will reduce the wavelength interrogation noise. According to the wavelength interrogation noise Equation (1):

$$\lambda_c - \bar{\lambda} = \frac{\sum_i (\lambda_i - \bar{\lambda}) I_i}{\sum_i I_i} \quad (1)$$

From Equation (1), it can be seen that the wavelength interrogation noise (N_λ) mainly originates from the detected optical intensity (I_i) noise, and the optical intensity noise is mainly composed of shot noise. At this point, the optical intensity noise away from

the resonance wavelength dominates the wavelength interrogation noise (N_λ). Therefore, higher spectral depth and lower background noise at off-resonance will significantly reduce the centroid wavelength interrogation noise (N_λ), specifically, please refer to Refs. [1-2].

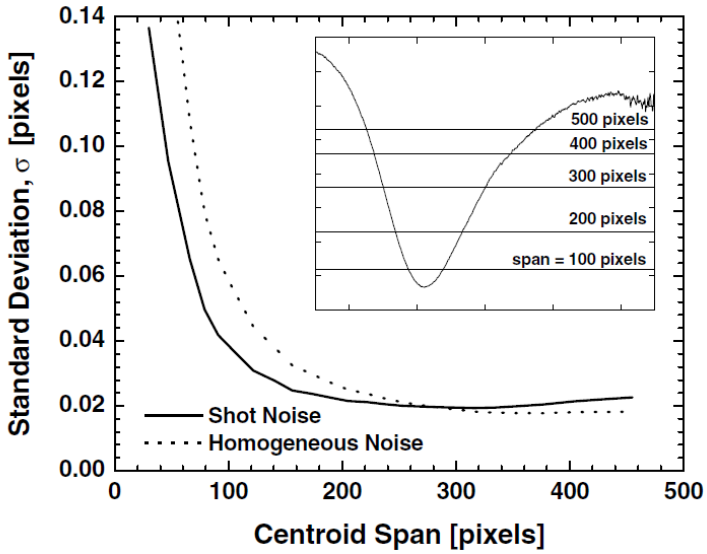

Fig. S6. Predicted centroid wavelength noise levels for sensor spectra for different centroid span (or threshold) sizes. The predicted models are the realistic shot noise model (noise increases with intensity) and the homogeneous noise model (light-independent noise), respectively[3].

It should be noted that in practical engineering applications, the threshold (η) needs to be determined and selected according to the actual situation. Specifically, Ref.[3] can provide a preliminary explanation to illustrate this phenomenon. As in Fig. S6, for the same spectrum, the higher the centroid span (or threshold) in a given range, the more accurate the calculation of its centroid wavelength is (because there are more pixel point counts in the spectrum participating in the centroid calculation, which statistically plays a greater averaging role). However, the higher the centroid span (or threshold), the statistical advantage of increasing the number of samples is offset by the increased noise level of the high-intensity pixels far from the center of resonance[3]. As a result, there is a slight increase in noise at the centroid wavelength at this point. Based on the results in Fig. S6, the centroid span(or threshold) is generally selected to be close to 300 pixels, and the noise of the centroid wavelength interrogation is at a lower level[3]. Therefore, there is a compromise in setting the size of the threshold (η) in a particular measurement system.